Employing SAFT coarse grained force fields for the molecular simulation of thermophysical and transport properties of CO_2 – n-alkane mixtures

Lingru Zheng[1], Fernando Bresme[2], J.P. Martin Trusler[1] and Erich A. Müller[1,*]
[1] Department of Chemical Engineering, Imperial College London, U.K.,
[2] Department of Chemistry, Imperial College London, U.K.

Abstract

We report an assessment of the predictive and correlative capability of the SAFT coarse-grained force field as applied to mixtures of CO_2 with n-decane and n-hexadecane. We obtain the pure and cross interactions parameters by matching simulations to experimental phase equilibrium behavior and transfer these parameters to predict shear viscosities. We apply both equilibrium (based on the Green-Kubo formulation) and non-equilibrium (based on the application of an external force to generate an explicit velocity field) algorithms. Single and two-site models are explored for CO_2 and, while for volumetric properties both models provide good results, only the model that aligns with the molecular shape is found to be robust when describing highly asymmetric binary mixtures over wide ranges of temperature and pressure. While the models provide good quantitative predictions of viscosity, deviations amongst the algorithms and with experimental data are encountered for binary mixtures involving longer chain fluids, and in particular at high-pressure and low-temperature states.

Introduction

Fluid mixtures comprising carbon dioxide (CO_2) and n-alkanes are frequently encountered in the petrochemical industry, with applications in supercritical extraction[1], CO_2 sequestration[2] and enhanced oil recovery[3], to name just a few. An accurate description of their phase behavior and transport properties, and in particular shear viscosities, is crucial for the optimal design of physicochemical processes. While phase behavior and viscosities can be measured experimentally[4,5,6,7] calculating these properties "*in silico*" has the benefit of providing insights at the microscopic level, as well as enabling the exploration of extreme temperatures and pressures that are difficult to access experimentally. To some extent, modern equations of state provide this capability, but there are limitations in terms of their predictive nature, extrapolation to high temperatures and pressures, and they fail to provide a universal framework for both volumetric, interfacial and transport properties[8]. Molecular simulation, on the other hand, provides an avenue to tackle this challenge in a consistent manner.

* Author to whom correspondence should be addressed; e.muller@imperial.ac.uk

Dissimilarities in size, shape and polarity between CO_2 and n-alkanes impose challenges to modelling. For instance, apart from the usual dispersion interaction, CO_2 has a permanent quadrupole moment and a relatively small size which imparts unique thermophysical properties, whereas n-alkanes molecules are essentially uncharged and apolar but have significant length-to-breadth ratios. The mixture of CO_2+n-alkanes is hence both energetically and entropically asymmetrical, leading to highly non-ideal behavior. Mixtures of CO_2+n-alkane start to display limited liquid-liquid miscibility as the alkane carbon number exceeds six [9]. Shorter alkanes, up to dodecane[10], exhibit Type II phase behavior[11] where a continuous path joins the critical points of the pure components. The vapor-liquid-liquid equilibrium locus extends from a quadruple point towards the upper critical end point (UCEP). For alkanes longer than tetradecane, the mixture displays Type III phase behavior with two critical lines: one extending from the critical point of the pure alkane (the less volatile component) towards high pressures; and the other extending from the critical point of CO_2 (the more volatile component) to the UCEP[12]. While traditional cubic equations of state (EoSs) are widely used in predicting such phase behaviour, they have the disadvantages of accounting only for near-spherical components (hence being increasingly less suited to describe longer alkanes) and thus requiring many empirical parameters to describe the cross-interactions in mixtures[13]. On the other hand, molecular-based EoSs such as the statistical associating fluid theory (SAFT)[14,15,16], and in particular the third-generation versions[17,18], are particularly suited to account for the asymmetries in these mixtures. SAFT has been used successfully to predict fluid phase behavior and even the transition of CO_2 + alkanes from type II to type III phase behavior as the carbon number increases[19].

Given the exponential growth of available computational resources[20], the previously perceived advantages of algebraic EoSs are reduced and as the demand for more realistic and precise description of fluid systems grows[21], computational simulations such as molecular dynamics (MD) became increasingly relevant in this space. These modelling tools provide an exact numerical description of fluid systems and allow both thermodynamic and transport properties to be assessed once the force field is specified[22]. Using molecular simulations to compute transport properties such as viscosities is not without its limitations: large uncertainties in statistics, complexities in solving autocorrelation functions and weak signal to noise ratio are frequent issues[23,24]. This manuscript tests an available coarse-grained force field in its capacity to provide accurate predictions for the CO_2-n-alkane mixtures.

Regardless of the modelling strategy, the predictive capacity of any molecular simulation is constrained by the transferability, reproducibility and robustness of the intermolecular potential employed. A number of force fields have been developed and tested for modelling pure CO_2, n-alkane and their mixtures. These force fields are broadly classified into all-atom (AA), united-atom (UA) and coarse-grained (CG) force fields. AA force fields, as their name suggests, provide characterization parameters for each and every atom in the system, the covalent bonds and angle

potentials. On the other hand, UA force fields involve lumping the carbon atoms with their corresponding hydrogens and treating them as individual interaction centers. Further grouping of atoms (*e.g.* to the average of three heavy atoms and the corresponding hydrogens) is made when converting into a CG representation. It is beyond the remit of this manuscript to review the state of the art and to compare the different models available. Discussions in the introduction sections of ref. 25 and ref. 26 provide an overview of the state of the art of molecular models for alkanes and CO_2.

Most popular force fields will provide reasonable predictions of the volumetric properties of both pure alkanes and CO_2. It is in the extension to the modelling to transport properties where some questions arise, since this represents an extrapolation and a strong test of the validity of the force fields. A recent blind test of models[27], aimed precisely at determining capabilities in this area, concluded that the viscosity of a small branched alkane could be predicted reliably at pressures up to 1 GPa, although slightly underestimating the experimental results. This confirms the results of Mondello and Grest[28] who compared the performance of UA potentials against a modified UA potential with shifted centers of mass (AUA) for modelling viscosities of n-decane and n-hexadecane using both EMD (Green-Kubo) and NEMD algorithms. They found that the optimized AUA model produced results 21-28% lower than experimental data for n-decane and 45-88% lower for n-hexadecane at 298 K. Here, the lower bound corresponds to the results when using EMD algorithm and the upper bound corresponds to the use of NEMD algorithm. On predicting viscosities using NEMD for hydrocarbons, a similar study[29] evaluated the efficacy of AA and UA potentials as well as their heterogeneous version with optimized potentials of liquid simulations (OPLS). It is found that UA models tend to underestimate viscosity whereas AA force field tends to overestimate viscosity by more than 20% over six hydrocarbon systems. Further, the prediction worsens when the bonds connecting atoms are treated as rigid. Following this trend, one would expect that CG models would fare worse. It is often stated that CG models are inherently incapable of representing transport properties, as they smear out the molecular details which cause the "friction" between particles. This contribution scrutinizes the extent to which this latter statement is true and explores the extent to which viscosity can be predicted using typical CG models parametrized on the basis of volumetric properties and phase behavior only.

The SAFT CG force field

Parameters for CG force fields are often obtained by systematically removing unwanted degrees of freedom of a detailed model, a procedure known as a "bottom-up" approach. Independent of the strategy of integration, the parameters obtained by the bottom-up approach are often state-dependent. This is not a flaw in the CG procedure but rather a result of focusing on a single or limited number of state points and obtaining local minima in an otherwise very complex optimization procedure. In contrast, a "top-down" approach has been adopted by the developers of the SAFT force field where the intermolecular potential parameters are estimated directly via

fitting an analytical Equation of State (*e.g.* the SAFT-γ Mie[17,18]) against a range of thermophysical properties. The key to the process is the accurate representation of the underlying Hamiltonian, which guarantees a one-to-one relation between the force field parameters and the corresponding macroscopic properties.

The SAFT coarse grained force fields are based on Mie intermolecular potentials, $u(r)$, for spherical isotropic beads, which can be represented as

$$u(r) = C\,\varepsilon\left[\left(\frac{\sigma}{r}\right)^{\lambda_r} - \left(\frac{\sigma}{r}\right)^{\lambda_a}\right] \tag{1}$$

where

$$C = \left(\frac{\lambda_r}{\lambda_r - \lambda_a}\right)\left(\frac{\lambda_r}{\lambda_a}\right)^{\lambda_a/(\lambda_r - \lambda_a)} \tag{2}$$

In this equation, r is the center-to-center distance between two spherical beads, λ_r and λ_a are parameters that control the steepness of the repulsion and the overall shape and range of the attractive part of the potential, σ is the length scaling parameter, and ε is the minimum depth of the potential well. Individual beads (which in a CG model represent several atoms in a molecule) may be connected in linear chains of m beads

The one-to-one link between the parameters that govern the analytical SAFT EoS and those that define the SAFT force field allows several avenues to be taken to obtain the optimal "effective" parameters for a given substance. The most obvious approach is to perform a least-squares fit of the EoS parameters to a selection of experimental data to find the best "compromise" parameters. While many types of data can be used, fitting to vapor pressures and saturated liquid densities along the coexistence curve, but avoiding the near critical region, has been seen to provide consistent and reliable data. Avendaño et al.[26] first illustrated this parameterization procedure for CO_2 against the prementioned three coarse-graining criteria - representability, transferability and robustness, before extending to pure n-alkanes[30]. Inspection of the EoS through a corresponding states approach suggests that, apart from the number of coarse-grained segments or beads (m), there are three degrees of freedom corresponding to the size scale (σ), energy scale (ε) and the overall shape or range of the potential which is a unique function of one of the two exponents, normally λ_r, once the other is fixed. The independent specification of both a repulsive and attractive exponent in the Mie potential was recognized by Ramrattan et al.[31] to be redundant. Therefore, in principle, the scaling of only three variables to corresponding properties of the target fluid is sufficient to define the EoS parameters. This is the pathway taken by Mejía et al.[32] and Herdes et al.[33] who proposed correlations to find σ, ε and λ from a saturated density, the critical temperature and Pitzer's acentric factor respectively. One can also recognize a direct influence of the exponent λ_r on the length of the coexistence curve, i.e. on the ratio between the critical- and triple-point

temperatures, an issue which has been addressed by Ramrattan et al.[31], suggesting the use of a simple linear correlation which can be used to obtain models that guarantee a close match of the triple and critical points. All of the above mentioned pathways provide for different parameter values with variations in the observed quality of the fits in the diverse regions of the phase space. It becomes important in this context to understand what properties are optimized and/or which parameter results in the best compromise.

The degree of coarse-graining expressed as the number of effective beads utilized to represent a molecule is found to have an influence on the numerical values of the parameters. In this case, a close match to the actual geometry of the target molecule suggests an improved match to structural, and eventually, macroscopic properties [34,35] . SAFT CG models for carbon dioxide, for instance, include both one-bead and two-bead representations. Despite its simplicity, the single-bead model of Avendaño[26] can accurately predict a wide range of thermophysical properties that were not used during parameterization. Examples include the enthalpy of vaporization, interfacial tension, subcooled and supercritical densities, and second-derivative thermodynamic properties such as speed of sound, heat capacity, isothermal compressibility, thermal and Joule-Thomson expansion coefficient. Comprehensive studies have shown that the Avendaño parametrization for CO_2 is competitive with atomistic models for the prediction of volumetric properties although the largest deviations are seen in the prediction of viscosities [36,37,38]. A two-bead model for CO_2, on the other hand, would provide for a closer match to the molecular shape which would suggest an improved representation of the thermophysical properties that depend on the molecular details (e.g. diffusion, viscosity). Parameters for a dimer CO_2 and longer chain n-alkanes model have been provided by Herdes et al.[Error! Bookmark not defined.]. An essentially equivalent dimer CO_2 model, developed by Rahman[39] by fitting the SAFT equation of state to experimental vapor pressure and saturated liquid density data from the triple point up to 90% of the critical temperature, is employed here. Jaeger et al.[40] observed improved results for the bulk viscosity of CO_2 when employing these two-site models.

Finally, an item for consideration for chain fluids is the appropriate accounting of the intramolecular degrees of freedom. The SAFT EoS has no provision for including these effects, hence they have to be inferred from higher-fidelity models at the quantum or atomistic level. Results from fitting sophisticated SAFT heteronuclear models for alkanes suggest that the inter-bead vibration and flexibility have little effect on volumetric properties but are important for interfacial and transport properties [25] e.g. understanding the diffusion of long alkanes and waxes at low temperatures[41]. In summary, Table 1 presents the models and force field parameters for fluids encountered in this study. Potential interactions at cutoff at 2 nm and no long range corrections are included in the calculations[42]. This rather long cutoff is employed to maintain the internal consistency between the force field parameters and the SAFT theory used to parametrize the models.

For binary mixtures, the equation (1) and (2) are also applied to the cross-interactions, with the following combining rules:[17]

$$\sigma_{ij} = \frac{\sigma_{ii} + \sigma_{jj}}{2} \tag{3}$$

$$\varepsilon_{ij} = (1 - k_{ij}) \frac{\sqrt{\sigma_{ii}^3 \sigma_{jj}^3}}{\sigma_{ij}^3} \sqrt{\varepsilon_{ii} \varepsilon_{jj}} \tag{4}$$

$$\lambda_{ij} = 3 + \sqrt{(\lambda_{ii} - 3)(\lambda_{jj} - 3)} \tag{5}$$

Here, the subscripts *ii* and *jj* refer to pure-component parameters , while the *ij* subscript refers to the cross interactions. A binary interaction parameter (k_{ij}) is included to modulate the energy cross interactions. It is expected to take a non-zero value for CO_2-alkane interactions[43] to cover the disparity between the quadrupolar attractions included in the dispersion interactions between the CO_2 pairs and the non-polar nature of the alkanes.

Table 1 Inter- and intra-molecular SAFT-γ CG Mie force field parameters. For pure components: *m* represents the number of CG beads, σ is the average bead size, ε represents the energy scale of the potential well; λ_r and λ_a are the repulsive and attractive exponents respectively. For binary mixtures, combining rules given in Eq. 3-5 are used to compute the unlike interaction parameters σ_{ij}, ε_{ij}, $\lambda_{r,ij}$ and $\lambda_{a,ij}$. Within a molecule, k_{bond} and k_{angle} are the bond and angle spring constants respectively; at bond length r_0 and angle θ_0, the harmonic potential reaches the equilibrium point.

Intermolecular parameters – like interactions						
Component	Source	*m*	σ [nm]	ε/k_B [K]	λ_r	λ_a
CO_2	(a) Avendaño et al.[26]	1	0.3741	353.55	23.00	6.66
	(b) Rahman [39]	2	0.2850	190.14	13.77	6.00
n-decane	Herdes et al. [33]	3	0.4584	415.19	20.92	6.00
n-hexadecane	Herdes et al. [33]	5	0.4432	418.13	21.20	6.00
Intermolecular parameters – unlike interactions						
Components (*i* + *j*)			σ_{ij} [nm]	ε_{ij}/k_B [K]	$\lambda_{r,ij}$	$\lambda_{a,ij}$
CO_2 (a)+ n-decane			0.4163	377.25	21.93	6.31
CO_2 (a)+ n- hexadecane			0.4087	380.37	22.08	6.31
CO_2 (b)+ n-decane			0.3717	258.35	16.89	6.00
CO_2 (b)+ n- hexadecane			0.3641	262.24	17.00	6.00
Intramolecular parameters[25]						
Component	k_{bond} [kJ.mol^{-1}.nm^{-2}]		r_0 or σ [nm]	k_{angle} [kJ.mol^{-1}.rad^{-2}]		θ_0
CO_2 (a)	-		-	-		-
CO_2 (b)	15000		0.2850	-		-
n-decane	6309.5		0.4584	22.18		157.6

n-hexadecane	6309.5	0.4432	22.18	157.6

(a) Refers to the one-bead model of CO_2 ; (b) Refers to "dimer" or two-bead model of CO_2

In the SAFT force field described here, beads are spherical and linked at a distance of σ, however, this is a condition that can be relaxed[44]. For chains of beads, an intramolecular potential consisting of harmonic bond stretching u_{bond} and bond-angle bending u_{angle} contributions is employed:

$$u_{\text{bond}} = \frac{k_{\text{bond}}}{2}(r - r_0)^2 \tag{6}$$

$$u_{\text{angle}} = \frac{k_{\text{angle}}}{2}(\theta - \theta_0)^2 \tag{7}$$

where k_{bond} and k_{angle} are the spring constants for the bond stretching and bond-angle bending potential, respectively, r_0 is the bond length constant corresponding to the minimum (equilibrium position) of the harmonic potential and is equal to σ for molecules made up of homonuclear segments. Finally, θ_0 is the equilibrium angle formed by three neighboring beads. The inter- and intra-molecular bonding parameters used in this work are given in Table 1. All bead-bead non-bonded interactions are included in the calculations.

Simulation details

Vapor-liquid equilibrium

Phase equilibria is calculated using a direct method, where the two coexisting phases along with the two explicit interfaces are modelled[45]. We fill a rectangular box with a fixed number of molecules of one or both components such that a phase split at sub-critical temperatures will be observed, *i.e.* at a density within the spinodal envelope. For pure component systems, we use a simulation box of 1:1:3 height:width:length ratio. Periodic boundary conditions are employed in all Cartesian directions. The elongation promotes the formation of the interfaces and allows the vapor-liquid separation to be clearly observed in the simulation box. For two binary mixtures, (CO_2 + n-decane) and (CO_2 + n-hexadecane), boxes of width to length ratios at 1:5 and 1:4 are used respectively to accommodate thicker interfacial regions (see Fig. 1). The number of molecules employed for pure CO_2, n-decane and n-hexadecane systems is 5000, 3000 and 2000 separately, and a total of 6000 molecules are employed for (CO_2 + n-decane) system and 4000 molecules for (CO_2 + n-hexadecane) system.

Classical molecular dynamics simulations are performed in the canonical ensemble, keeping the number of particles (N), the system volume (V) and temperature (T) fixed. We chose to use the GROMACS[46] simulation suite (version 5.1.3) to compute vapor-liquid equilibria, although in the

Supporting Information (SI) we present an evaluation of the accuracy of the software as compared to other alternatives: *DL_POLY* 4.09.02[47], *ms2*[48] (employing the *NPT* ensemble with chemical potential calculated via Widom insertion method, together known as the NPT+μ method), and MedeA®-GIBBS (9.6.2)[49] (employing Gibbs Ensemble Monte Carlo simulations). Throughout, the same set of SAFT CG force field parameters (the dimer CO_2 model) are used to warrant a fair comparison and validation. A table summarizing these results can be found in the SI, where different software suites show systematically different results even after taking into account the expected fluctuations and errors in the simulations. These types of divergences, product of both systematic and statistical errors, are reminiscent of experimental measurements[50]. For internal consistency, we use GROMACS (2018) to produce all further results.

Initial high-temperature runs are undertaken to ensure appropriate mixing of the systems and after quenching to the specified temperature, the systems are left for 1 ns to equilibrate and run for another 3 ns to collect data. The time step is fixed at 0.01 ps and the temperature is controlled using the Nosé-Hoover thermostat with a 2 ps time constant. To eliminate the need for long-range correction terms for pressure and energy, throughout all simulations, the potential is truncated at 2nm (roughly 4~7σ depending on the molecular type). Once the system is quenched, the density (and/or composition) of a specific phase can be obtained by averaging the density profile of that phase across the simulation box, discarding the interfacial region. An illustration of an equilibrated simulation box and density profiles for a pure two-bead model CO_2 system are given in Fig. 1. The vapor pressure at each temperature is obtained by simulating under the canonical ensemble a single-phase box that has the same gas phase density as the two-phase box.

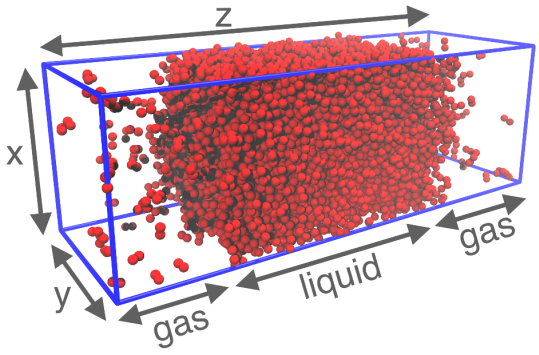

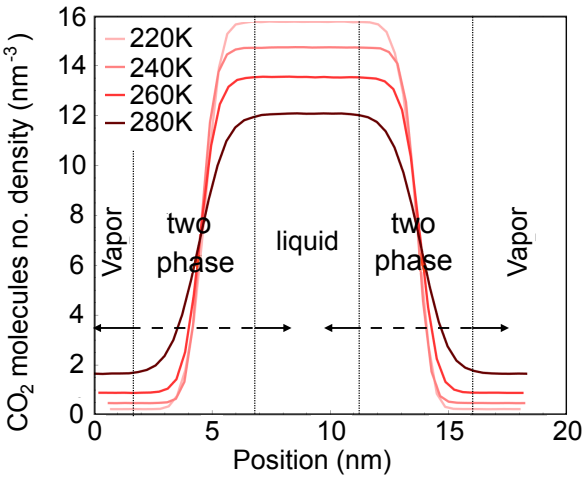

Figure 1 Top: Snapshot of an equilibrium configuration used to determine the vapor-liquid equilibria of CO_2. Simulation box contains 5000 two-bead model CO_2 molecules, represented as red beads, showing vapor-liquid coexistence at 240 K. Bottom: Density composition profiles along the box, indicating the vapor, liquid and interfacial regions at 220 K, 240 K, 260 K and 280 K. The densities are recorded as the number of CO_2 molecules per nm^3 for each case; the values are plotted against the positions along the length (z) of each simulation box.

Viscosity

To predict shear viscosities, two complementary algorithms are employed in this work based on either evaluating the pressure fluctuations in equilibrium molecular dynamics (EMD) or performing periodic shear perturbations in non-equilibrium molecular dynamics (NEMD)[51]. EMD evaluates the Green-Kubo[52,53] relation directly[22, 54] linking the shear viscosity to the equilibrium correlation of fluctuating pressure:

$$\eta = \frac{V}{k_B T}\int_0^{\infty}\left\langle P_{ij}(t)P_{ij}(t+\tau)\right\rangle d\tau \qquad (8)$$

where V is the system volume, and P_{ij} are the off-diagonal elements of the pressure tensor, *i.e.* $i \neq j$; their values being recorded during MD simulations as a function of time t. In Eq. 8, the integrand represents the autocorrelation function (ACF) of the off-diagonal components of the pressure tensor with respect to a time delay τ. In the end, integration is applied to the time-dependent autocorrelation results computed before; solving from t = 0 to $t = \infty$ to give η.

In practice, the recorded pressure component values often exhibit strong oscillations. We mitigate these fluctuations in two ways. First, we remove the invariant part of the pressure components built-up during the simulation by employing the normalized autocorrelation function (ACF) Eq. 9, where

$$\left\langle P_{ij}(t)P_{ij}(t+\tau)\right\rangle = \frac{1}{n_{\max}}\sum_{\tau=0}^{\tau_{\max}}\left((P_{ij}(t)-\overline{P}_{ij})\,(P_{ij}(t+\tau)-\overline{P}_{ij})\right) \tag{9}$$

where $\overline{P_{ij}}$ is the average of P_{ij} over the correlation interval. Second, we follow the recommendations of Maginn et al. [55,56] to repeat the simulation up to 40 times and fit the average results with a double exponential function Eq.10. Finally, the viscosity is read from the fit at the time when the corresponding averaged normalized ACF first decays to zero.

$$\eta(t) = A\alpha\tau_1(1-e^{-t/\tau_1}) + A(1-\alpha)\tau_2(1-e^{-t/\tau_2}). \tag{10}$$

For determining viscosity, a cubic simulation box is employed, and the system is compressed under the isobaric-isothermal *NPT* ensemble for 2 ns until reaching the specified pressure. An appropriate configuration (which provides for the specified temperature and pressure) is used as starting configuration for subsequent simulations EMD and NEMD simulations.

When running the EMD, the system is simulated under the *NVT* ensemble for 5 ns using a 2 fs time step, with the energy values recorded at every step. To improve the statistics, we carry out this *NVT* simulation up to 40 times, resulting in 40 independent trajectories. The generated statistics are then used in pressure fluctuations which involve direct computation of Green-Kubo in Eq. 8 (labelled as EMD for the rest of this study). We carry out the post-processing outside of GROMACS by removing the first 1ns production run and retaining the rest 4ns for each of the 40 trajectories. The time-varying off-diagonal pressure tensor components are stored as P_{xy}, P_{xz} and P_{yz} for each simulation. The average viscosity is then obtained using Eq. 11. We compute the corresponding standard deviation σ_η by fitting its running value against a power law given in Eq. 11 and read at the time the average viscosity starts to level off

$$\sigma_\eta^{GK}(t) = Bt^b \tag{11}$$

where A, B, b, α, τ_1, τ_2 are the fitting parameters. The standard deviation value is read at the time the averaged ACF first reaches zero.

While the perturbations in pressure fluctuations are intrinsic, an external force is applied to the system to generate a more tangible response when using periodic perturbations method in NEMD. This external force can thereby be added as a macroscopic acceleration term in the Navier-Stokes equations using a cosine , $\zeta\cos(k_z z)$, assuming only the flow direction (z) velocity and acceleration are non-zero and a function of z only. Here $k_z = 2\pi/l_z$ represents the wave vector and l_z is the box length in z direction. Hence, the velocity profile can be written as:

$$U_x(t,z) = \zeta \frac{\rho}{k_z^2 \eta}(1 - e^{-t/\tau_H})\cos(k_z z) \quad (12)$$

In this equation, $\rho/k_z^2\eta$ can be written as τ_H, known as the hydraulic time constant, representing the relaxation time of the plane waves travelling in the fluid. In MD, acceleration can be added to each step, hence an average of the pre-factor $\zeta(\rho/k_z^2\eta)$ in Eq. 12 is tuned to obtain the value of the viscosity η[51].

During the NEMD simulations, the selected configurations are also simulated under the canonical *NVT* ensemble at a 2 fs interval for 2 ns at more than 6 different cos-acceleration amplitudes (ζ), each with three repetitions. The amplitudes are often chosen to be lower than 0.1 nm.ps^{-2} to avoid shear thinning or thickening. The viscosity is outputted as "1/viscosity" via the g_energy subroutine from GROMACS[51]. We average the three data points at each acceleration and apply a weighted linear fit to the averaged data points on the viscosity versus acceleration graph. The weights at each acceleration are set to be inversely proportional to the statistical viscosity errors σ_η^{NEMD} calculated by Eq. 13 [51]. The intercept of this weighted linear fit is read as the final viscosity.

$$\sigma_\eta^{NEMD} = \frac{2}{s_{\max}}\sqrt{\frac{k_B T \eta}{V t_a}} \quad \text{where} \quad s_{\max} = \zeta \frac{\rho}{\eta k_z} \quad (13)$$

In Eq. 13, t_a is the time over which the average velocity is determined, s_{max} is the maximum shear rate and ζ is the value of acceleration in nm.ps^{-2}.

Neither the EMD nor the NEMD algorithms are without limitations[57, 58]. The former suffers from the need to appropriately evaluate the ACF, as to not include unnecessary noise, while the results of the latter strongly depend on the applied driving force. We compare results from both methodologies without prejudice.

Results

Pure fluids

CO_2

The results for the predicted vapor pressure and saturated liquid density for both the one-bead[26] and the two-bead model[39] of CO_2 are shown in Fig.2.

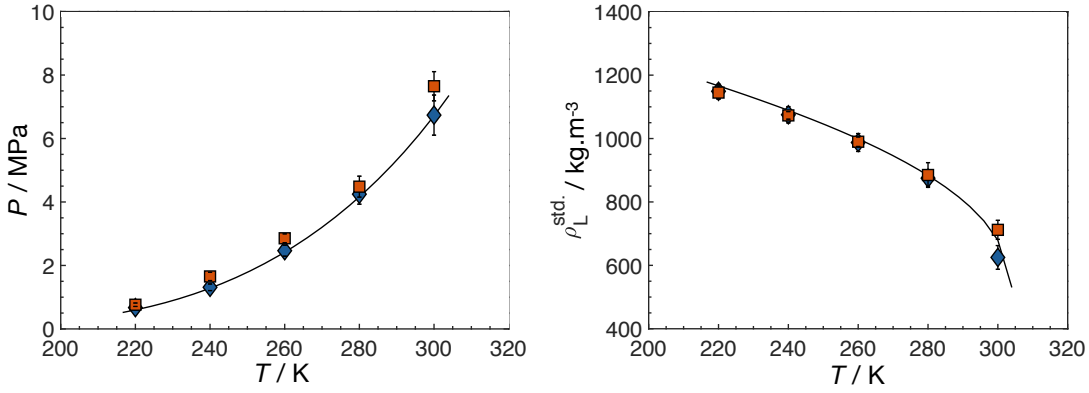

Figure 2 Vapor pressures and saturation liquid densities for pure CO_2 as compared to smoothed experimental data[59] (solid line). MD simulation results for the one bead (squares) and two bead (rhombi) models are shown.

The one-bead model used here was fit to the critical temperature and liquid density at the expense of a poorer adjustment to the vapor pressure. The two-bead model, on the other hand, represents both the pressure and liquid density well but at the cost of over-predicting the critical temperature. Both these fitting strategies are evident as small discrepancies between MD simulation results and experimental measures in Fig. 2.

Systems containing 5000 CO_2 molecules are simulated at 10 MPa and at temperatures from 220 K to 300 K to obtain liquid phase shear viscosities. The simulated viscosities and the smoothed experimental data are plotted in Fig. 3.

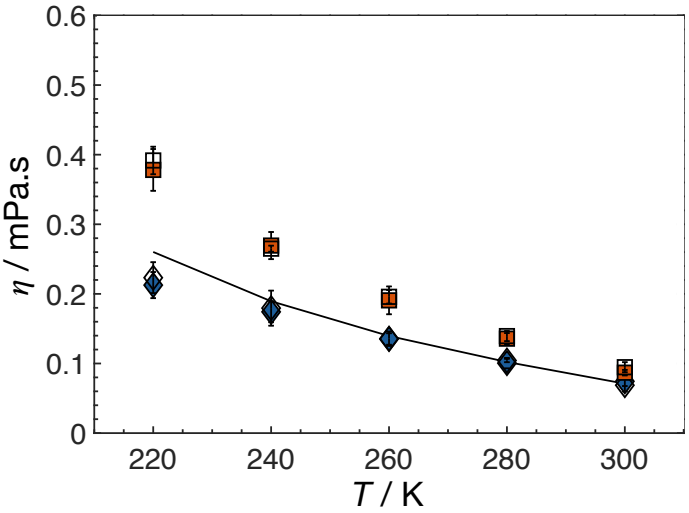

Figure 3 Shear viscosity of the two-bead model CO_2 (rhombi) and the one-bead model CO_2 (squares) computed at 10 MPa from 220K to 300K using EMD (filled symbols), and NEMD (empty symbols) as compared to smoothed experimental data[60] (solid line).

Despite both models representing volumetric properties accurately, there are significant differences in the prediction of viscosities. The inclusion in the coarse grain model of a shape that is closer to the underlying molecule seems to be the defining factor for the improved viscosity predicted by the two-bead model. A slight under-prediction is seen at low temperatures, most likely due to the mismatch (of this parametrization) between the experimental solid-fluid transition temperature and that of the molecular model. The average absolute deviation (%AAD) of the simulation results in contrast to the smoothed experimental data is presented Table S1 of the Supporting Information. We have investigated how the rigidity of CO_2 bonds (for the dimer model) affects the shear viscosity by setting the bond strength k_{bond} to a significantly large value. The resulting viscosities (not shown) suggests that the model is insensitive towards the bond strength. A similar observation is also made in Nieto-Draghi et al.'s work on transport properties of CO_2 [61].

n-decane and n-hexadecane

n-decane is represented by a homonuclear three-bead model, while n-hexadecane is represented by a five-homonuclear-bead model; their non-bonded interaction parameters are given in Table 1. Within their respective boxes, 3000 n-decane molecules are simulated while 2000 n-hexadecane molecules are simulated. Box dimensions are included as SI. Fig. 4 shows the comparison between the simulated vapor pressures or saturation densities and the smoothed experimental data of n-decane[62] and n-hexadecane[63,64].

The volumetric properties of the alkanes seem well represented by the models used. No appreciable differences are found in the thermodynamic properties when segments are rigidly bonded as compared to softly bonded results in Fig.4, and this is consistent with the previous observations on the behaviour of SAFT models[25]. The vapor pressure plots in Fig.4 reveal that the simulations deviate noticeably from experimental data at high pressures close to the critical point.

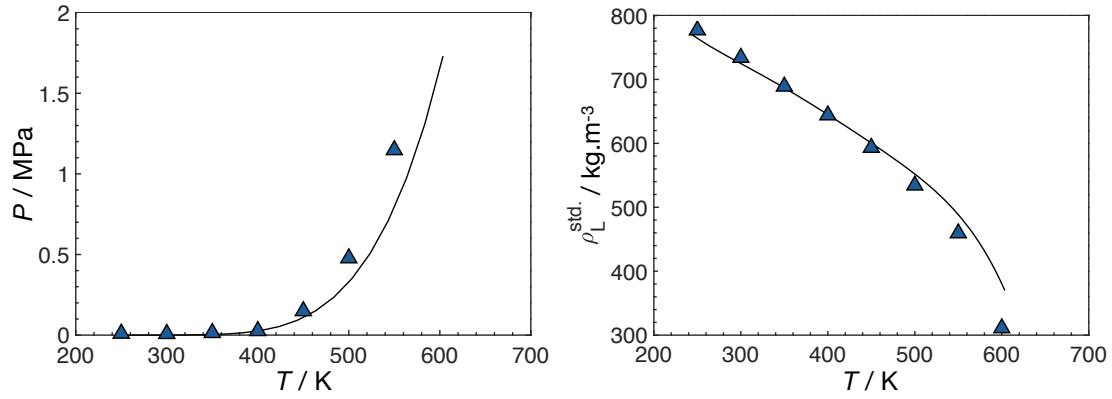

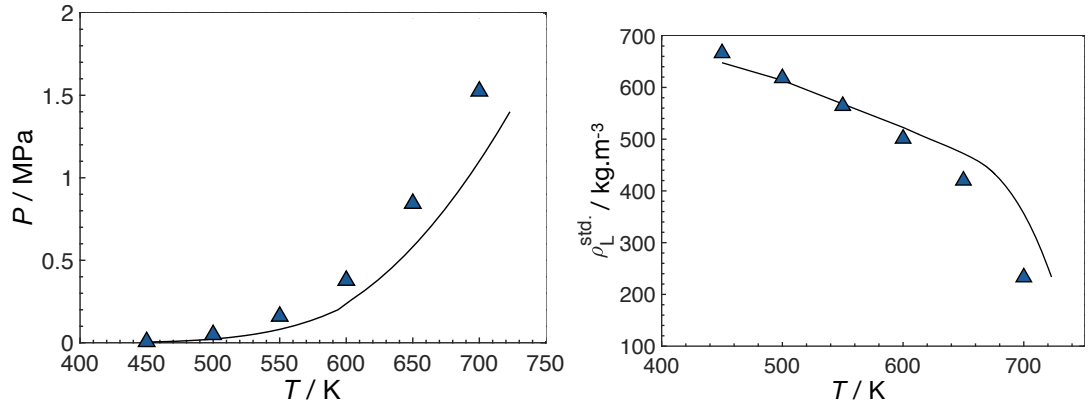

Figure 4 MD simulation results (triangles) for the vapor pressures and saturation liquid densities for n-decane (top) and n-hexadecane (bottom) as compared to their corresponding smoothed experimental data[62-64] (solid line). Errors are the size of the symbols.

Using 3000 n-decane molecules, we examine the viscosities at 10 MPa and 60 MPa, at temperatures from 319 K to 470 K. The computed shear viscosities are plotted against experimental data[65] in Fig. 5. Also included in Fig. 5 are the n-hexadecane viscosities, obtained following the same simulation procedure with 2000 molecules. The fluid contained in the cubic simulation box remain as a liquid from 333.15 K to 413.15 K at two distinct pressures, 6.9 MPa and 62.05 MPa. These computed shear viscosities are plotted against experimental data[66]. In all cases, the agreement between the experimental and simulation data is excellent and of a quantitative nature.

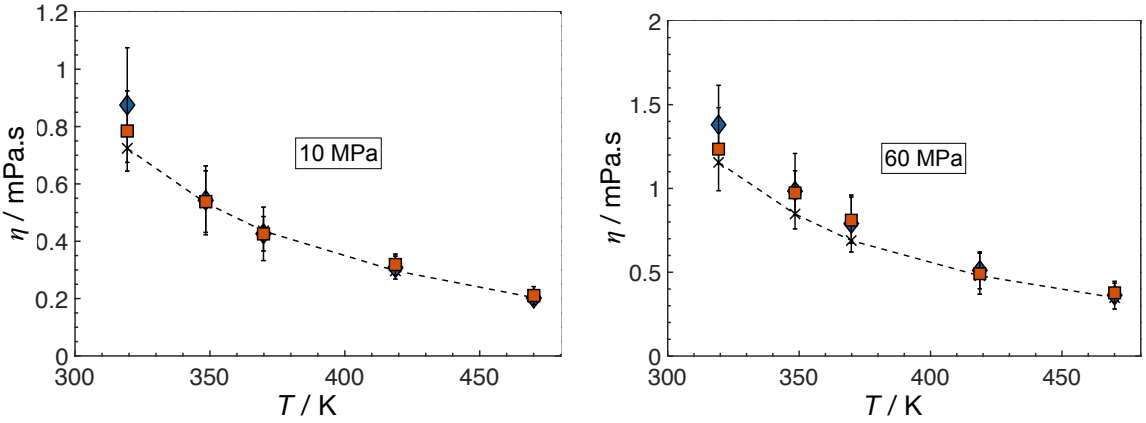

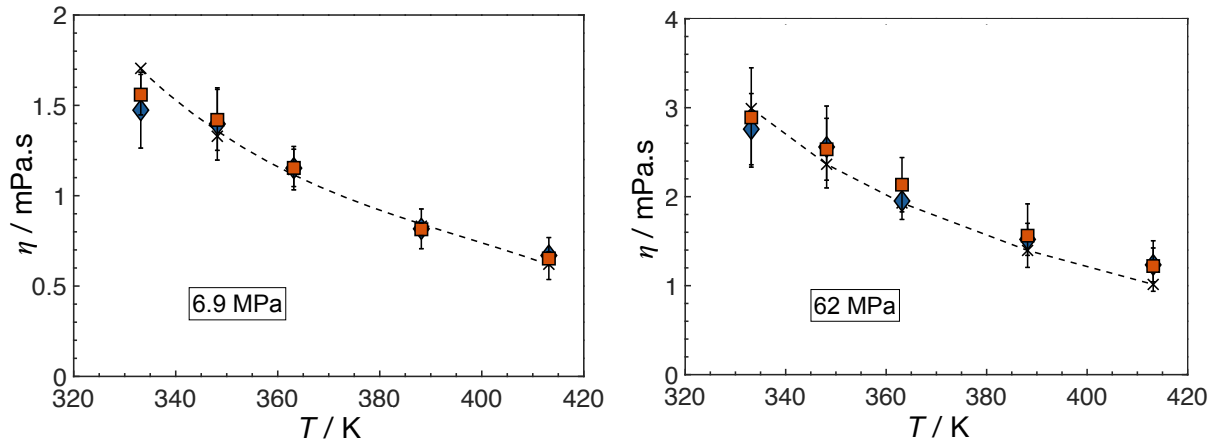

Figure 5 Shear viscosity of n-decane (top) computed at 10 MPa (left) and 60 MPa (right) and n-hexadecane (bottom) computed at 6.9 MPa (left) and 60 MPa (right) computed using EMD (rhombi), and NEMD (squares) as compared to experimental data (crosses, dashed lines are a guide to the eye)[65,66].

As in the case of CO_2, we study how the intramolecular potential parameters, k_{bond} and k_{angle}, affect the mixture viscosity over various temperatures at low and high pressures. The n-decane and n-hexadecane molecular models used to generate results in Fig. 5 comprise of 3 and 5 homonuclear beads respectively, and can stretch and bend following an harmonic potential with constants tabulated in table 1. In the rigid case, k_{bond} is set at 15000 kJ.mol^{-1}.nm^{-2} and k_{angle}, at 150 kJ.mol^{-1}.rad^{-2}. In both scenarios we fix θ_0 at 157.6° and r_0 equal to the corresponding σ. Such change in intramolecular potential imposes insignificant effects on the viscosities (hence not shown).

We notice that the autocorrelation function (ACF) of n-decane and n-hexadecane presents oscillations during relaxation, and the amplitudes tends to grow larger as the intramolecular bonds become "softer". This is the case even when the ACF is averaged over 90 trajectories (30 simulation runs × 3 off-diagonal pressures for each simulation run). A comparison between two averaged ACF for CO_2 and n-hexadecane is shown in Fig. 6. Datasets are selected under conditions where the ACF gives the fastest decay of the respective systems. As can be seen, the decay of ACF for n-hexadecane is delayed by an order of magnitude in time as compared to CO_2. This requires one to compute viscosity from a longer running integral and emphases the importance of using the normalized ACF (Eq.9) to remove the invariant pressure contributions accumulated by the oscillations of the ACF. Furthermore, the discrepancy between computed viscosities and experiments is closely correlated to the accuracy with which the density of n-hexadecane is modelled[67,68]. When comparing the simulated densities of n-hexadecane with experimental data[69] we found that deviations are more apparent at high pressures and low temperatures.

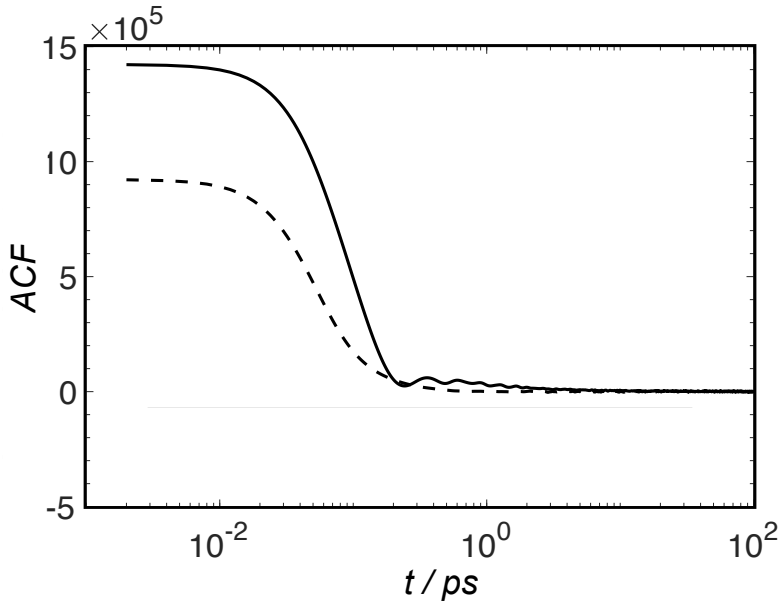

Figure 6 Autocorrelation function (ACF) computed for CO_2 at 300 K, 10 MPa (dashed line) and n-hexadecane at 420 K, 6.9 MPa (solid line).

The accurate prediction of critical properties of the pure components is crucial to obtain meaningful results for the high temperature VLE states of mixtures. Here we determine the critical temperature (T_c), pressure (P_c) and density (ρ_c) from critical scaling laws (detailed in the SI), and compare them with respect to the experimental critical values in Table 2. It can be seen that the one-bead CO_2 model underestimates the critical temperature, while overestimates the critical pressure and densities as shown before in Fig. 2. Both the n-decane and n-hexadecane model underpredict the T_c and overpredict P_c significantly. Therefore, significant deviations from the experiments appear in the vicinity of critical points in Fig. 4.

Table 2 Experimental and simulated critical properties for CO_2, n-decane and n-hexadecane computed using critical scaling laws.

Properties	Components	2-bead CO_2	1-bead CO_2	n-decane	n-hexadecane
T_c /K	Expt.	304.1		617.7	722.0
	Simulation	304.7	300.0	599.5	700.0
P_c /MPa	Expt.	7.37		2.10	1.40
	Simulation	7.30	7.40	2.96	2.04
ρ_c /(kg.m^{-3})	Expt.	468		233	219
	Simulation	464	487	233	215

(CO_2 + n-decane) binary mixture

The simulation of binary mixtures follow similar protocols as employed for pure components. For CO_2 + n-decane system, the simulation box is filled with n-decane and CO_2 at a molecular ratio such that the average composition lies within the two-phase region. The detailed settings of the simulation boxes at various objective pressures are included in SI. The system is ran for 1ns and equilibrated for 4ns under the *NVT* ensemble at 0.01ps time step. By the end of each simulation, the density data for both components are collected to construct a pressure-composition (P-xCO_2) diagram as given in Fig.7. The discrepancy between experiments and MD simulations imply that a simple combining rule is inadequate for generating accurate force field parameters between CO_2 and n-decane. n-alkane interactions are dominated by van der Waals (dispersion) forces, while CO_2-CO_2 interactions result from a sum of both dispersion forces and those related to the permanent quadrupole forces. Mie fluid models make no separation of these interactions and treat all CG attractions through a single term. Hence, the cross-interaction needs to be modulated by a binary interaction parameter k_{ij} to correct for the disparity between the van der Waals forces which dominate the interactions between pure n-alkanes and the permanent quadrupolar forces which influence amongst CO_2 molecules. We choose a k_{ij} value at 0.08, corresponding to a cross interaction ε/k_B = 237.69 K between the two-bead (dimer) CO_2 and n-decane or ε/k_B = 347.07 K between the one-bead (mono) CO_2 and n-decane, that provide for a close match between the simulations and the VLE experimental data. In principle, one could invoke the use of the SAFT EoS to fit the interaction parameters, as was done in closely related approaches[70,43], however the theory fails to accurately reproduce the critical region for these state points, providing for spurious results.

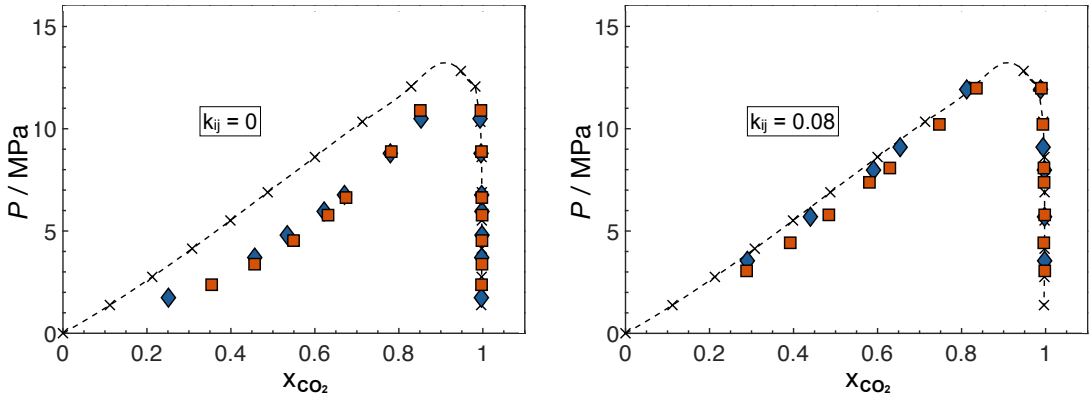

Figure 7 Effect of incorporating a binary interaction parameter, k_{ij}, in the phase equilibria of CO_2 - n-decane mixture VLE. Pressure-composition relation for (CO_2 + n-decane) at 344 K using either a two- site CO_2 model (rhombi) or one-site CO_2 model (squares). The experimental measurements[71] are shown as crosses (connected by dashed lines as a guide to the eye). The left diagram corresponds to the scenario where no k_{ij} is employed; the right corresponds to k_{ij} = 0.08. Error bars are smaller than the symbol size.

We further examine the prediction of the viscosity for the mixture CO_2 + n-decane using either the one- or two-bead models for CO_2, and compare the simulated data with experimental reference

from Cullick and Mathis[72] (Fig.8). The binary mixture viscosities are tested at four temperatures and each under a lower and a higher pressure. While data at various CO_2 compositions (x_{CO_2}) are available, we choose to study x_{CO_2} at 0.505, for if x_{CO_2} is close to 0 or 1, we expect the results to converge to the pure n-decane or pure CO_2. The thermodynamic conditions under which the simulations are carried out are listed in Table 3. To make up the desired composition, 2024 CO_2 molecules and 1984 n-decane molecules are inserted into cubic simulation box. Following the discussion above, a k_{ij} of 0.08 is used to adjust the cross-interactions as it provides a closer description to the experimental vapor-liquid equilibria at 344K.

Table 3 Temperature and pressure conditions under which the shear viscosity simulations are performed, and compared to experimental data for CO_2 + n-decane system[72].

T /K	**311.21**	**343.18**	**373.36**	**403.30**
P_{low} /MPa	7.12	6.93	10.60	11.58
P_{high} /MPa	30.94	27.58	27.75	27.99

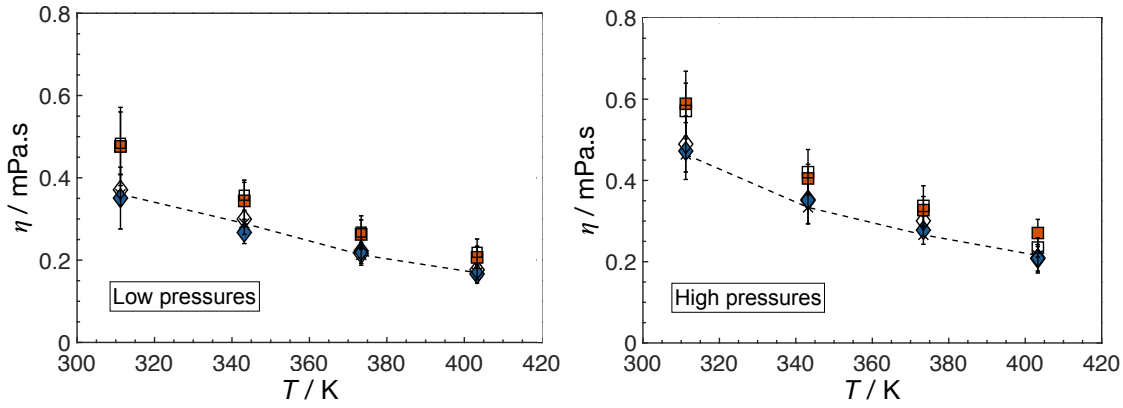

Figure 8 Shear viscosities of CO_2-n-decane computed at relatively low (left) and high (right) pressures from 311.21 K to 403.3 K . Symbols are the two-site (dimer) CO_2 (rhombi) and single-site CO_2 model (squares). The pressures at different temperatures are listed in Table 4. Experimental measurements[72] are shown in crosses (guided by dashed lines) as compared to EMD (filled symbols) and NEMD (empty symbols) results.

(CO_2 + n-hexadecane) binary mixture

Simulations for CO_2 + n-hexadecane mixture are carried out at 298.4 K and 323.2 K. At these conditions, and for particular densities, the system is expected to have a Type III phase behaviour experiencing regions of liquid-liquid equilibrium (LLE) at low-temperature which terminate at an upper critical endpoint (UCEP) at high pressures. We have employed a binary interaction parameter of k_{ij} = 0.1 to correct the cross-interactions between two-site (dimer) CO_2 and n-hexadecane, corresponding to a cross-interaction ε/k_B = 236.02 K, which is similar to the value

employed for two-site CO_2-decane mixtures, suggesting that in these models it is the absolute cross parameter which is the value that is transferrable (rather than the value of the binary interaction parameter). As a note in passing, we should point out that both the decane and hexadecane models are homonuclear in nature; the effective beads represent an average effective interactions. In opposition to this, more sophisticated SAFT models for alkanes differentiate between groups of atoms that form the ends (-CH_2-CH_2-CH_3) and middle (-CH_2-CH_2-CH_2-) alkane moieties, in these cases, one would expect more transferability between the cross parameters of smaller and longer alkanes. Similarly, a k_{ij} = 0.1 is needed to adjust the cross-interactions between the one-bead CO_2 and n-hexadecane to provide a better description of the experimental data. This corresponds to a ε/k_B = 349.94 K, again, very close to the absolute value of one-bead CO_2 + n-decane interactions. Shown in Figure 9 are the pressure versus CO_2 composition plots at 298.4 K and 323.2 K. The results of simulations using k_{ij} = 0 are presented in the SI and show a diminished fit to the experimental data[73,74].

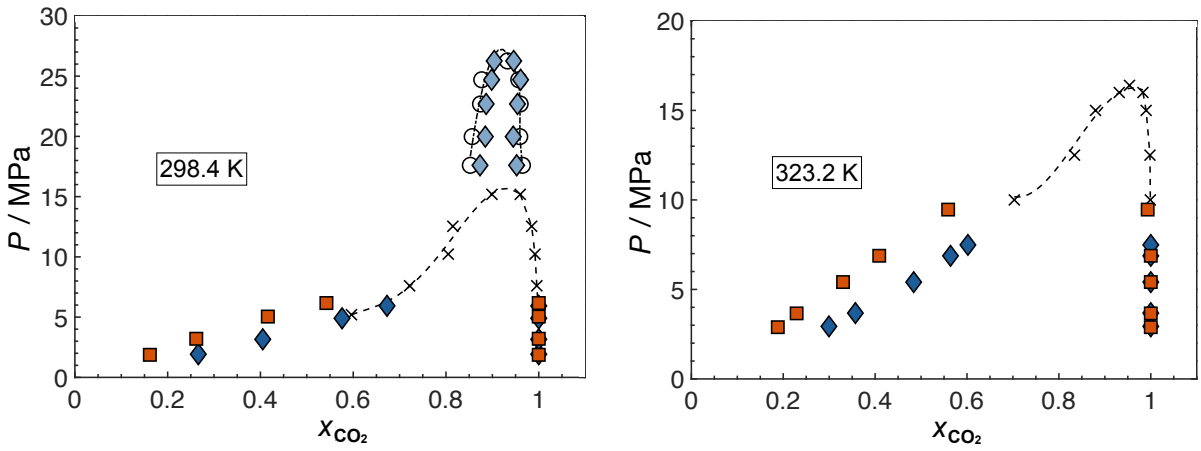

Figure 9 Pressure-composition relation for (CO_2 + n-hexadecane) at 298.4 K (left) and 323.2 K (right) using either a two-site (dimer) plotted as rhombi or one-site (mono) CO_2 model plotted as squares. The vapor-liquid equilibrium (VLE) experimental measurements[73,74] are shown as crosses (connected by dashed lines as a guide to the eye). A binary interaction parameter of k_{ij}=0.1 is used in all cases. The liquid-liquid equilibrium (LLE) experimental measurements[73] are shown as circles, guided by dash-dotted lines, and the simulation results using a two-site (dimer) CO_2 model within the LLE region is plotted using light color filled rhombi. Error bars are smaller than the symbol size.

Liquid-liquid equilibria (LLE) is obtained through MD simulation by employing the $NP_{zz}T$ ensemble, where the number of molecules, temperature and the longitudinal pressure of the system are kept constant. It is observed that the two-site (dimer) CO_2 - n-hexadecane system can reach a stable LLE state at P $\geq$ 6.4 MPa, whilst below 6.3 MPa the system becomes unstable. This is consistent with the transition pressure measured[75] at 298.13 K for CO_2 + n-hexadecane, where vapor-liquid-liquid equilibrium occurs at 6.304 MPa. The LLE region is hence explored using the

dimer CO_2 at 298.4 K and the simulation results are plotted in the top diagram of Figure 9, and compared to experimental measurements[73]. It is remarkable that the simulation model is able to reproduce LLE without the need of re-adjusting parameters. A close-up snapshot of the LLE interface is provided in figure 10 and shows an interfacial region that spans approximately 2 nm and a clear clustering of molecules in both coexisting phases.

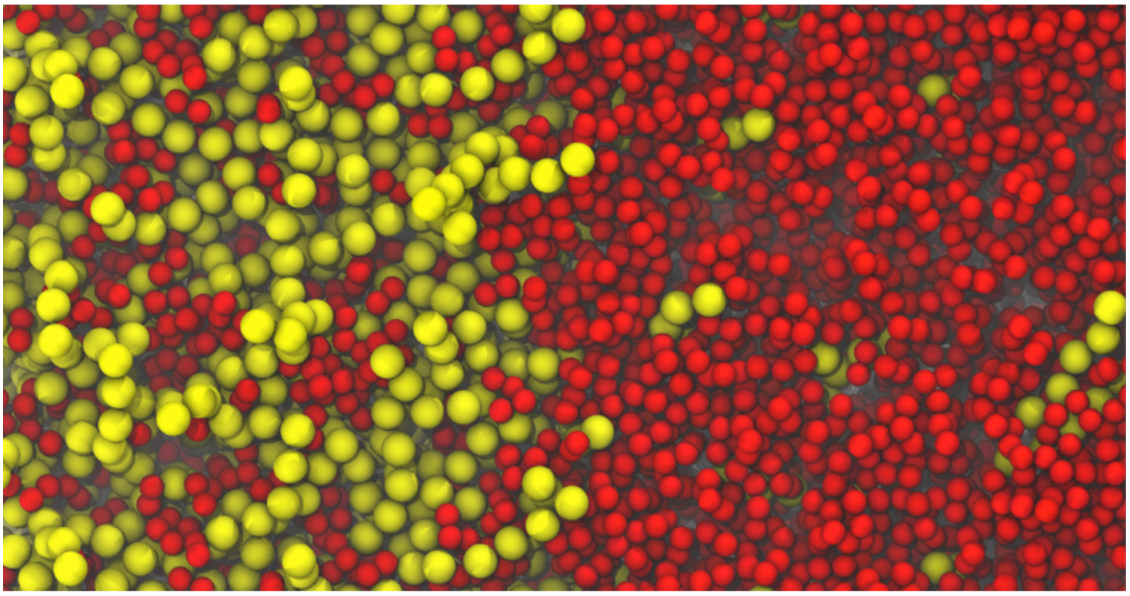

Figure 10 Snapshot detailing a section of the liquid-liquid interfacial region between a mixture of the two-bead model of CO_2 (red beads) and n-hexadecane (yellow beads) at 298.4 K and 7 MPa.

To evaluate the performance of the prediction of the mixture viscosity, the simulations data is compared to reference experimental data taken from Mohammed et al.[76] at three different CO_2 fractions: 0.0690, 0.5877 and 0.7270. Similar to CO_2 - n-decane systems, we focus here on computing shear viscosities when x_{CO_2} is close to 0.5. Thereby, a box containing 1800 CO_2 and 1263 n-hexadecane molecules are simulated to give a CO_2 fraction of 0.5877. We use $k_{ij} = 0.1$ for all cases, which provided for the closest match to volumetric properties. Viscosity data were measured experimentally under the conditions listed in Table 4.

Table 4 Temperature and pressure conditions under which the shear viscosity simulations are performed, and compared to experimental data CO_2 + n-hexadecane system

T /K	**298.18**	**323.15**	**373.11**	**423.11**	**473.15**
P_{low} /MPa	10.44	10.63	20.76	25.91	43.72
P_{high} /MPa	40.38	60.11	80.24	118.17	120.61

At each temperature, the system viscosity was studied at two different pressure levels (as specified in Table 4), one corresponding to a relatively low (< 50 MPa) and the other relatively high (> 40 MPa). We present the viscosities as a function of temperature at these low and high pressures in Fig.11. There is a slight deviation between algorithms at low temperatures and high pressures. It is evident from the figure that the single-site CO_2 model over predicts of viscosities in contrast to the two-site CO_2 model which provides for a quantitative representation of the viscosity.

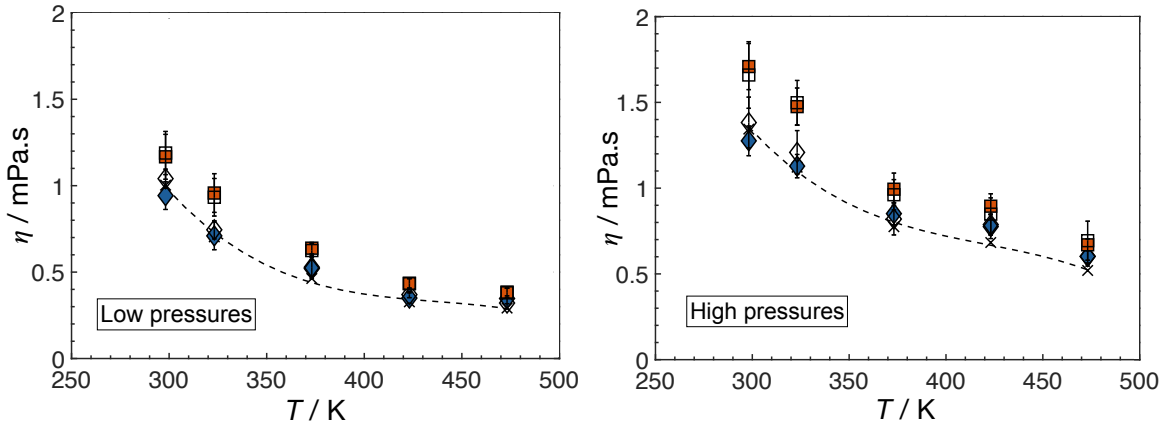

Figure 11 Shear viscosities of CO_2-n-hexadecane computed at relatively low (left) and high (right) pressures from 298.18 K to 473.15 K dimer CO_2 (rhombi) and single-site CO_2 model (squares). The pressures at different temperatures are listed in Table 4. Experimental measurements[76] are shown in crosses (guided by dash lines) as compared to EMD (filled symbols) and NEMD (empty symbols) results.

Conclusions

The results suggest that SAFT coarse-grained models parametrized by the top-down approach, where macroscopic VLE data is employed to obtain the molecular force fields parameters, have sufficient transferability to be used to evaluate viscosities for mixtures of CO_2 and alkanes. The cross-interaction parameters, fitted against phase-equilibrium data are found to be transferrable to viscosity predictions, even for mixtures at high pressures and temperatures.

The two-site CO_2 model, while almost indistinguishable to the one-site model in its ability to predict pure fluid properties, provides a more accurate prediction of viscosity. It is in the prediction of mixture phase equilibria and in the prediction of viscosities that the alignment between the molecular shape and the molecular model representation seems to be important. Comparing to experiments, in all cases, the discrepancies between the calculated viscosities and the experiments

can be attributed to the difficulties of the models in capturing the system density or phase transition point precisely.

In terms of computing viscosity, the results obtained show good agreement amongst the different algorithms when dealing with simple fluids at low pressures and high temperatures. Deviations are observed when involving longer chain fluids, binary mixtures and in particular at the high pressure and low temperature states, which coincide with states where the dynamics are slower. In these cases, the NEMD tends to provide systematically higher viscosity estimates as compared to the EMD, although the uncertainties in associated with the latter are larger. Even upon employing a normalized ACF, the EMD method converges slowly for long chain fluids and the computation of the off-diagonal elements of the microscopic pressure tensor for each trajectory prolongs the computation time of the ACF by an order of magnitude.

Supporting Information

Supporting Information is provided in a separate document. It includes a) Discussion of critical property estimation b) Comparison of simulation results for pure density and vapor pressures of several simulation suites using the dimer CO_2 model; c) numerical simulation results for the viscosity of CO_2 d) Dimensions of the simulation box sizes employed; e) the pressure-composition plots of CO_2 + n-hexadecane using $k_{ij} = 0$.

Acknowledgements

We would like to express our gratitude towards Shell Global Solutions for funding this project and their active engagement in the "Digital Rocks" research program. We would like to thank Alin Marin Elena, Jadran Vrabec and Marianna Yiannourakou for their effort in providing the DL_POLY 4.09, ms2 and MedeA®-GIBBS (9.6.2) simulated phase equilibrium data using our dimer CO_2 model. E.A.M. acknowledges support from EPSRC through research grants to the Molecular Systems Engineering group (Grant Nos. EP/E016340, EP/J014958 and EP/R013152). We are grateful to the UK Materials and Molecular Modelling Hub for computational resources, which is partially funded by EPSRC (Grant No. EP/P020194/1)

References

[1] McHugh, M.; Krukonis,V. *Supercritical fluid extraction: principles and practice*; Elsevier: Amsterdam, 2013

[2] Smit, B.; Reimer, J.A.; Oldenburg, C.M.; Bourg, I.C. *Introduction to carbon capture and sequestration*; Imperial College Press: London, 2014

[3] Alvarado, V.; Manrique, E. Enhanced Oil Recovery: An Update Review. *Energies* **2010**, *3*, 1529–1575.

[4] Reamer, H.H.; Sage, B.H. Phase equilibria in hydrocarbon systems. volumetric and phase behavior of the n-decane-CO2 system. *J. Chem. Eng. Data* **1963**, *8*, 508–513.
[5] Charoensombut-Amon, T; Martin, R.J.; Kobayashi, R. Application of a generalized multiproperty apparatus to measure phase equilibrium and vapor phase densities of supercritical carbon dioxide in n-hexadecane systems up to 26 MPa. *Fluid Phase Equilibria* **1986**, *31*, 89–104.
[6] van der Steen, J. de Loos, Th. W.; de Swaan Arons, J. The volumetric analysis and prediction of liquid-liquid- vapor equilibria in certain carbon dioxide+ n-alkane systems. *Fluid Phase Equilibria* **1989**, *51*, 353–367.
[7] Mohammed, M.; Ciotta, F.; Trusler, J.P.M. Viscosities and densities of binary mixtures of hexadecane with dissolved methane or carbon dioxide at temperatures from (298 to 473) K and at pressures up to 120 MPa. *J. Chem. Eng. Data* **2017**, *62*, 422-439.
[8] Kontogeorgis, G.M.; Folas, G.K. *Thermodynamic Models for Industrial Applications: From Classical and Advanced Mixing Rules to Association Theories*; Wiley: New York, 2010.
[9] Im, U.K.; Kurata, F. Heterogeneous phase behavior of carbon dioxide in n-hexane and n-heptane at low temperatures. *J. Chem. Eng. Data* **1971**, *16*, 412-415.
[10] van der Steen, J.; de Loos, Th.W.; de Swaan Arons, J. The volumetric analysis and prediction of liquid-liquid-vapor equilibria in certain carbon dioxide+n-alkane systems. *Fluid Phase Equilibria* **1989**, *51*, 353–367.
[11] Scott, R.L.; van Konynenburg, P.H . Static properties of solutions. van der Waals and related models for hydrocarbon mixtures. *Discuss. Faraday Soc.* **1970**, *49*, 87–97.
[12] Schneider, G; Alwani, Z; Heim, W.; Horvath, E.; Franck, E.U. Phasengleichgewichte und kritische erscheinungen in binären mischsystemen bis 1500 bar, CO2 mit n-octan, n-undecan, n-tridecan und n-hexadecan. *Chemie Ing. Tech.* **1967**, *39*, 649–656.
[13] Cismondi, M.; Rodríguez-Reartes, S.B.; Milanesio, J.M.; Zabaloy, M.S. Phase equilibria of co2+ n-alkane binary systems in wide ranges of conditions: Development of predictive correlations based on cubic mixing rules. *Ind. Eng. Chem. Res.* **2012**, *51*, 6232–6250.
[14] Chapman, W.G.; Gubbins, K. E.; Jackson, G.; Radosz, M. SAFT: Equation-of-state solution model for associating fluids. *Fluid Phase Equilibria* **1989**, *52*, 31–38.
[15] Müller, E. A.; Gubbins, K. Molecular-based equations of state for associating fluids: A review of SAFT and related approaches. *Ind. Eng. Chem. Res*. **2001**, 40, 2193–2211.
[16] McCabe C.; Galindo, A. SAFT associating fluids and fluid mixtures, in *Applied Thermodynamics of Fluids* Ed. Goodwin, A.R.H.; Sengers, J.V.; Peters, C.J. RSC: London, 2010.
[17] Lafitte, T.; Apostolakou, A.; Avendaño, C.; Galindo, A.; Adjiman, C.S. ; Müller, E.A. ; Jackson, G. Accurate statistical associating fluid theory for chain molecules formed from Mie segments. *J. Chem. Phys.* **2013**, *139*, 154504.
[18] Papaioannou, V.; Lafitte, T.; Avendaño, C.; Adjiman, C. S.; Jackson, G.; Müller, E. A. ; Galindo, A. Group contribution methodology based on the statistical associating fluid theory for heteronuclear molecules formed from Mie segments. *J. Chem. Phys.* **2014**, *140*, 054107.
[19] Blas, F.J.; Galindo, A.. Study of the high pressure phase behaviour of CO2+ n-alkane mixtures using the SAFT-VR approach with transferable parameters. *Fluid Phase Equilibria* **2002**, *194*, 501–509.
[20] Szalay, A. ; Gray, J. 2020 computing: Science in an exponential world. *Nature* **2006**, *440*, 413.
[21] Barnard, A. S. In Silico Veritas. *ACS Nano* **2014**, *8*, 6520–6525.
[22] Allen, M. P.; Tildesley, D.J. *Computer simulation of liquids*. 2nd ed. Oxford University Press: Oxford, 2017.

[23] Palmer, B.J. Transverse-current autocorrelation- function calculations of the shear viscosity for molecular liquids. *Phys. Rev. E* **1994**, *49*, 359.
[24] Zhang,Y.; Otani, A.; Maginn, E. J. Reliable viscosity calculation from equilibrium molecular dynamics simulations: a time decomposition method. *J. Chem. Theory Comp.* **2015**, *11*, 3537–3546.
[25] Rahman, S.; Lobanova, O.; Jiménez-Serratos, G.; Braga, C.; Raptis, V.; Müller, E. A.; Jackson, G.; Avendaño, C.; Galindo, A. SAFT- γ Force Field for the Simulation of Molecular Fluids. 5. Hetero- Group Coarse-Grained Models of Linear Alkanes and the Importance of Intramolecular Interactions. *J. Phys. Chem. B* **2018**, *122*, 9161–9177.
[26] Avendaño, C.; Lafitte, T.; Galindo, A.; Adjiman, C.S.; Jackson, G.; Müller, E.A. SAFT-γ Force Field for the Simulation of Molecular Fluids. 1. A Single-Site Coarse Grained Model of Carbon Dioxide, *J. Phys. Chem. B* **2011**, *115*, 11154–11169.
[27] 10th Industrial Fluid Properties Simulation Challenge (http://fluidproperties.org/)
[28] Mondello, M.; Grest, G.S. Viscosity calculations of n-alkanes by equilibrium molecular dynamics. *J. Chem. Phys.* **1997**, *106*, 9327–9336.
[29] Allen, W.; Rowley, R. L. Predicting the viscosity of alkanes using nonequilibrium molecular dynamics: Evaluation of intermolecular potential models. *J. Chem. Phys.* **1997**, *106*, 10273-10281.
[30] Avendaño, C.; Lafitte, T.; Adjiman, C.S.; Galindo, A.; Müller, E.A.; Jackson, G. SAFT-γ Force Field for the Simulation of Molecular Fluids: 2. Coarse-Grained Models of Greenhouse Gases, Refrigerants, and Long Alkanes. *J. Phys. Chem. B* **2013**, *117*, 2717–2733.
[31] Ramrattan, N.S.; Avendaño, C.; Müller, E.A.; Galindo, A. A corresponding-states framework for the description of the Mie family of intermolecular potentials. *Mol. Phys*. **2015**, *113*, 932–947.
[32] Mejía, A; Herdes, C.; Müller, E.A. Force Fields for Coarse-Grained Molecular Simulations from a Corresponding States Correlation. *Ind. Eng. Chem. Res*. **2014**, *53*, 4131–4141.
[33] Herdes, C.; Totton, T.S.; Müller, E.A. Coarse grained force field for the molecular simulation of natural gases and condensates. *Fluid Phase Equilibria* **2015**, *406*, 91–100.
[34] T. Lafitte, T.; Avendaño, C.; Papaioannou, V.; Galindo, A.; Adjiman, C.S.; Jackson, G.; Müller, E.A. SAFT- γ force field for the simulation of molecular fluids: 3. Coarse-grained models of benzene and hetero-group models of n-decylbenzene. *Mol. Phys*. **2012**, *110*, 1189–1203.
[35] Müller, E.A.; Mejía, A. Extension of the SAFT-VR Mie EoS to model homonuclear rings and its parametrization based on the principle of corresponding states. *Langmuir* **2017**, *33*, 11518-11529.
[36] Aimoli, C.G.; Maginn, E.J.; Abreu, C.R.A. Force field comparison and thermodynamic property calculation of supercritical CO2 and CH4 using molecular dynamics simulations. *Fluid Phase Equilibria* **2014**, *368*, 80-90.
[37] Aimoli, C.G.; Maginn, E.J.; Abreu, C.R.A., Transport properties of carbon dioxide and methane from molecular dynamics simulations. *J. Chem. Phys.* **2014**, *141*, 134101.
[38] Aimoli, C.G.; Maginn, E.J.; Abreu, C.R.A., Thermodynamic Properties of Supercritical Mixtures of Carbon Dioxide and Methane: A Molecular Simulation Study. *J. Chem. Eng. Data* **2014**, *59*, 3041–3054.
[39] Rahman, S. *Development of coarse-grained models of ionic and non-ionic surfactants for the molecular simulation of structural, thermodynamic and dynamical properties*. PhD thesis, Imperial College London, 2016.
[40] Jaeger, F.; Matar, O.K.; Müller, E.A. Bulk viscosity of molecular fluids. *J. Chem. Phys*. **2018**, *148*, 174504–12.

[41] Shahruddin, S.; Jiménez-Serratos, G.; Britovsek, G.J.P.; Matar, O.K.; Müller, E.A. Fluid-solid phase transition of n-alkane mixtures: Coarse-grained molecular dynamics simulations and diffusion-ordered spectroscopy nuclear magnetic resonance. *Sci. Rep.*, **2019**, *9*, 1–9.
[42] Ibergay, C.; Ghoufi, A.; Goujon, F.; Ungerer, P.; Boutin, A.; Rousseau, B.; Malfreyt, P. Molecular simulations of the n-alkane liquid-vapor interface: Interfacial properties and their long range corrections. *Phys. Rev. E*, **2007**, *75*, 1–18.
[43] Lobanova, O.; Mejía, A.; Jackson, G.; Müller, E.A., SAFT-γ force field for the simulation of molecular fluids 6: Binary and ternary mixtures comprising water, carbon dioxide, and n-alkanes. *J. Chem. Thermodyn.* **2016**, *93*, 320–336.
[44] Walker, C.C.; Genzer, J.; Santiso, E. E. Development of a fused-sphere SAFT-γ Mie force field for poly(vinyl alcohol) and poly(ethylene). *J. Chem. Phys.* **2019**, *150*, 034901–16.
[45] Gelb, L.; Müller, E.A., Location of phase equilibria by temperature-quench molecular dynamics simulations. *Fluid Phase Equilibria* **2002**, *203*, 1–14.
[46] Abraham, M. J.; Murtola, T.; Schulz, R.; PaÍl, S.; Smith, J. C.; Hess, B.; Lindahl, E. GROMACS: High Performance Molecular Simulations Through Multi-Level Parallelism From Laptops to Supercomputers. *SoftwareX* **2015**, *1*, 19−25.
[47] Todorov, I.T.; Smith,W.; Trachenko, K.; Dove, M.T. DL_POLY_3: new dimensions in molecular dynamics simulations via massive parallelism. *J. Mat. Chem*. **2006**, *16*, 1911-1918.
[48] Rutkai, G.; Köster, A.; Guevara-Carrion, G.; Janzen, T.; Schappals, M.; Glass, C.W.; Bernreuther, M.; Wafai, A.; Stephan, S.; Kohns, M.; Reiser, S.; Deublein, S.; Horsch, M.; Hasse, H.; Vrabec, J. ms2: A molecular simulation tool for thermodynamic properties, release 3.0. *Comp. Phys. Comm.* **2017**, *221*, 343–351.
[49] Yiannourakou, M.; Ungerer, P.; Leblanc, B.; Ferrando, N.; Teuler, J.-M. Overview of MedeA®-GIBBS capabilities for thermodynamic property calculation and VLE behaviour description of pure compounds and mixtures: application to polar compounds generated from ligno-cellulosic biomass. *Molec. Sim.* **2013**, *39*, 1165-1211.
[50] Schappals, M.; Mecklenfeld, A.; Kröger, L.; Botan, V.; Köster, A.; Stephan, S.; García, E.J.; Rutkai, G.; Raabe, G.; Klein, P.; Leonhard, K.; Glass, C.W.; Lenhard, L.; Vrabec, J.; Hasse, H. Round Robin Study: Molecular Simulation of Thermodynamic Properties from Models with Internal Degrees of Freedom. *J. Chem. Theory Comput.* **2017**, *13*, 4270–4280 .
[51] Hess, B. Determining the shear viscosity of model liquids from molecular dynamics simulations. *J. Chem. Phys*. **2002**, *116*, 209–217.
[52] Green, M.S. Markoff random processes and the statistical mechanics of time-dependent phenomena. ii. irreversible processes in fluids. *J. Chem. Phys.* **1954**, *22*, 398–413.
[53] Kubo, R. Statistical-mechanical theory of irreversible processes. I. general theory and simple applications to magnetic and conduction problems. *J. Phys. Soc. Japan* **1957** *12*, 570–586.
[54] Evans, D.J.; Morriss, G. *Statistical Mechanics of Nonequilibrium Liquids*, 2nd ed.; Cambridge University Press: Cambridge, 2008.
[55] Zhang, Y.; Otani, A.; Maginn, E.J. Reliable viscosity calculation from equilibrium molecular dynamics simulations: a time decomposition method. *J. Chem. Theory Comp.* **2015**, *11*, 3537–3546.
[56] Maginn, E.J.; Messerly, R.A.; Carlson, D.J.; Roe, D.R.; Elliott, J.R.. Best practices for computing transport properties 1. self-diffusivity and viscosity from equilibrium molecular dynamics [article v1. 0]. *Living J. Comp. Molec. Sci*. **2018**, *1*, 6324.
[57] Tenney, C. M.; Maginn, E. J. Limitations and Recommendations for the Calculation of Shear Viscosity using Reverse Nonequilibrium Molecular Dynamics. *J. Chem. Phys*. **2010**, *132*, 014103.

[58] Jamali S. H.; Wolff, L. ; Becker, T. M.; de Groen, M.; Ramdin, M.; Hartkamp, R.; Bardow, A.; Vlugt, T. J. H.; Moultos, O. A. OCTP: A Tool for On-the-Fly Calculation of Transport Properties of Fluids with the Order-n Algorithm in LAMMPS. *J. Chem. Inf. Model*. **2019**, *59*, 1290–1294.
[59] Linstrom, P.J. ; Mallard, W.G. The NIST Chemistry WebBook: a chemical data resource on the internet. *J. Chem. Eng. Data* **2001**, *46*, 1059–1063.
[60] Fenghour, A.; Wakeham, W. A.; Vesovic, V. The viscosity of carbon dioxide. *J. Phys. Chem. Ref. Data* **1998**, *27*, 31-44.
[61] Nieto-Draghi, C.; de Bruin, Th.; Pérez-Pellitero, J.; Avalos, J.B.; Mackie, A.D. Thermodynamic and transport properties of carbon dioxide from molecular simulation. *J. Chem. Phys*. **2007**, *126*, 064509.
[62] Lemmon, E.W.; Huber, M.L. Thermodynamic properties of n-dodecane. *Energy Fuels* **2004**, *18*, 960-967.
[63] Salerno, S.; Cascella, M.; May, D.; Watson, P.; Tassios, D. Prediction of vapor pressures and saturated volumes with a simple cubic equation of state: Part I. A reliable data base. *Fluid Phase Equilibria* **1986**, *27*, 15-34.
[64]Yaws, C. L., Narasimhan, P.K. Critical properties and acentric factor—organic compounds. *Thermophysical properties of chemicals and hydrocarbons*. William Andrew Publishing: New York, 2009.
[65] Naake L.-D. *Die Viskosität von n-Dekan und Methan-Dekan Mischungen bei 300 °C und 3000 bar*. Ph.D. thesis, Universität Karlsruhe, 1984.
[66] Rajagopal, K.; Andrade, L.L.P.R.; Paredes, M.L.L. High-pressure viscosity measurements for the binary system cyclohexane + n-hexadecane in the temperature range of (318.15 to 413.15) K. *J. Chem. Eng. Data* **2009**, *54*, 2967-2970.
[67] Messerly, R.A.; Anderson, M.C.; Razavi, S.M.; Elliott, J.R. Improvements and limitations of Mie lambda-6 potential for prediction of saturated and compressed liquid viscosity. *Fluid Phase Equilibria*, **2019**, *483*, 101-115.
[68] Messerly, R.A.; Anderson, M.C.; Razavi, S.M.; Elliott, J.R. Mie 16-6 force field predicts viscosity with faster-than-exponential pressure dependence for 2,2,4-trimethylhexane. *Fluid Phase Equilib*ria, **2019**, *495*, 76–85.
[69] Amorim, J.A.; Chiavone-Filho, O.; Paredes, M.L.L.; Rajagopal, K. High-pressure density measurements for the binary system cyclohexane + n-hexadecane in the temperature range of (318.15 to 413.15) K. *J. Chem. Eng. Data* **2007**, *52*, 613–618.
[70] Mejía, A.; Cartes, M.; Segura, H.; Müller, E.A. Use of Equations of State and Coarse Grained Simulations to Complement Experiments: Describing the Interfacial Properties of Carbon Dioxide + Decane and Carbon Dioxide + Eicosane Mixtures. *J. Chem. Eng. Data* **2014**, *59*, 2928–2941.
[71] Reamer, H. H.; Sage, B. H. Phase Equilibria in Hydrocarbon Systems. Volumetric and Phase Behavior of the n-Decane-CO_2 System. *J. Chem. Eng. Data* **1963**, *8*, 508-513.
[72] Cullick, A. S.; Mathis, M.L. Densities and Viscosities of Mixtures of Carbon Dioxide and n-Decane from 310 to 403 K and 7 to 30 MPa. *J. Chem. Eng. Data* **1984**, *29*, 393-396.
[73] Scheidgen, A. *Fluid phase equilibria of binary and ternary carbon dioxide mixtures with hardly volatile organic substances up to 100 MPa. Cosolvency effect, miscibility windows and holes in the critical plane*. Ph.D. Thesis, Ruhr-Universität Bochum, 1997.
[74] Pöhler, H. *Fluidphasengleichgewichte binärer und ternärer Kohlendioxidmischungen mit schwerflüchtigen organischen Substanzen bei Temperaturen von 303 K bis 393 K und Drücken von 10 MPa bis 100 MPa*, Doctoral Thesis, Ruhr-Universität Bochum, 1994.

[75] van der Steen, J.; de Loos, Th. W.; de Swaan Arons, J. The volumetric analysis and prediction of liquid-liquid-vapor equilibria in certain carbon dioxide+n-alkane systems. *Fluid Phase Equilibria* **1989**, *51*, 353–367.
[76] Malami, M.; Ciotta, F.; Trusler, J.P.M. Viscosities and Densities of Binary Mixtures of Hexadecane with Dissolved Methane or Carbon Dioxide at Temperatures from (298 to 473) K and at Pressures up to 120 MPa. *J. Chem. Eng. Data* **2016**, *62*, 422-439.